Supplementary Materials

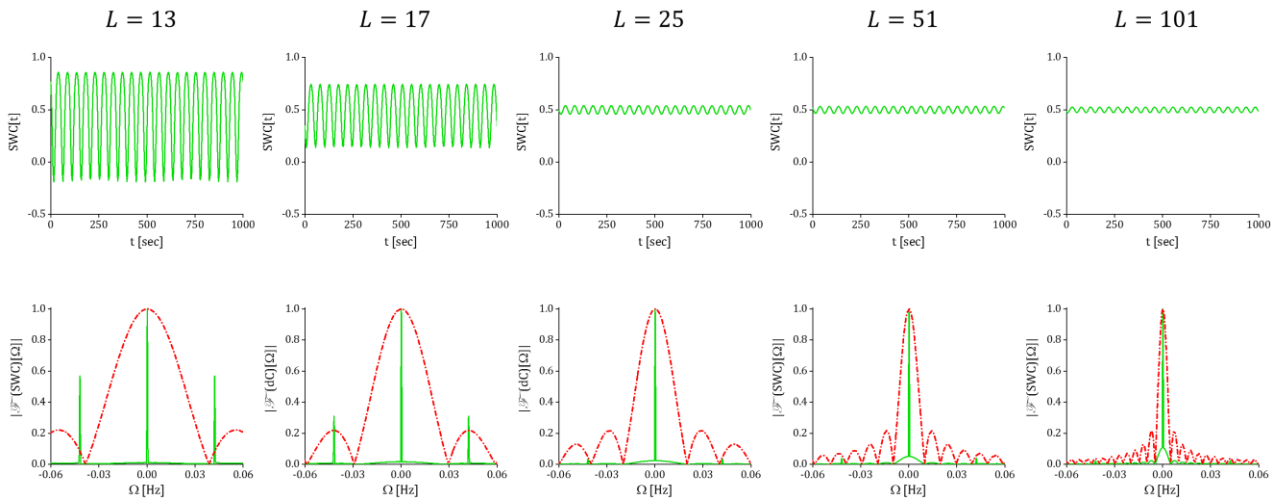

Figure S. 1. The SWC time series (the first row), and frequency spectrum (the second row), computed using rectangular window for the two time series $x = \cos(2\pi ft)$, and $y = \cos(2\pi ft + \varphi)$, where $f = 0.02$ and $\varphi = \pi/3$. Since these two time series fluctuate at the same frequency, they should show static correlation. However, sliding window connectivity analysis results in highly dynamic SWC series, for small window lengths, see first and second columns for $L \in \{13, 17\}$. This is also evident by the corresponding frequency spectrums in which a strong frequency component is present at 0.045 Hz. This is due to the fact that small window lengths do not allow estimating a reliable static measure for the time series mean and standard deviation which can affect the SWC coefficient measures. These fluctuations actually represent the alterations of the time series statistics over time, not the real dynamic correlations between the time series (referred to as spurious fluctuations). We saw that as window lengths increases, the SWC series approaches to a static series, while weak variations are still survived. Note that as the window length increases, the rate of the SWC change decreases, such that the difference between the SWC resulted from $L = 51$ and $L = 101$, is barely visible. Thus, for the time series with dynamic correlations, we need to choose the window length in order to make a balance in removing the spurious SWC fluctuations while maintaining the real dynamic correlations. The spurious fluctuations may not be removed completely for the fMRI time series that possess a wide-band frequency spectrum, as it would require longer windows that would eventually lead to static correlations. It is also worth mentioning that for this specific example of static correlation (having time series oscillating at a given frequency), one can completely eliminate the weak spurious fluctuations by choosing a window size equal to an integer multiplication of the time series period. Practically though, since fMRI time series are wideband signals, it is not possible to totally remove the spurious fluctuations from the SWC measures.

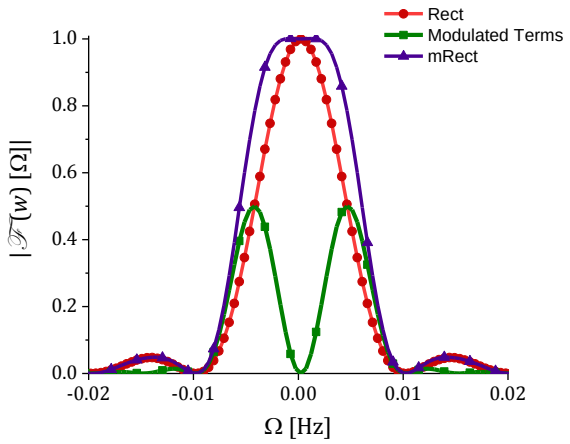

Figure S. 2. The rationale behind the proposed window function. The red curve shows the frequency spectrum of the conventionally used rectangular window with a cutoff frequency of $f_c = 0.01$ Hz. As we discussed in the main document, this window works as a low-pass filter. However, as opposed to an ideal filter which sharply drops at the cutoff frequency, its amplitude drops gradually as frequency increases. To compensate for this effect, we proposed adding a second term which is a modulated rectangular function that results in the green curve shown in the frequency domain. The modulation frequency is equal to the half of the cutoff frequency, i.e. $f_m = f_c/2 = 0.005$ Hz. The length of the resulting rectangular window is twice that of the original window which results in decreasing its bandwidth by a factor of 2. This combination results in two scaled sinc functions (the two green peaks that are centered at $\pm f_c/2$, with zeros occurring at 0 HZ and $\pm f_c$). By adding these two functions and tuning their relative parameters, i.e. amplitude and phase of the modulated terms as explained in the main document, one can compensate for the gradual drop of the rectangular function spectrum. This effect is shown in the purple curve.

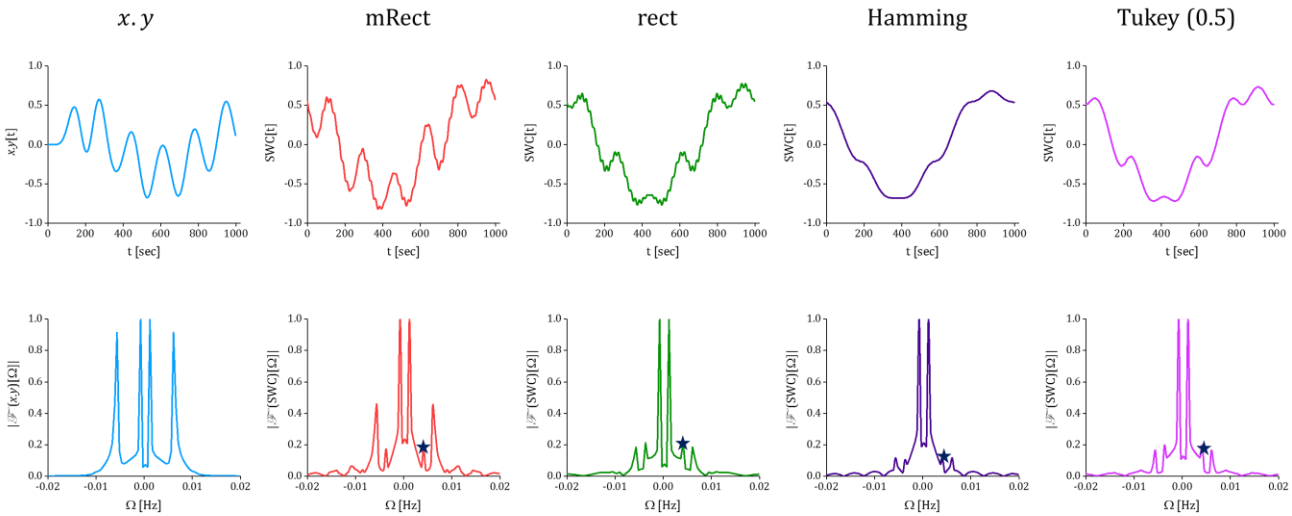

Figure S. 3. Pointwise multiplication and SWC time series and frequency spectrums with setting $L = 61$; the analysis was performed using the four window functions, with mRect window of length 121, rectangular window of length 61, Hamming window of length 121 and Tukey of length 91 time points. Comparing the SWC spectrums with those obtained using $L = 51$ time points (see Figure 3 in the main document) suggests that although amplitude of the spurious fluctuation at 0.004 is reduced by half, the real dynamic correlation occurring at $\delta f_2 = 0.006$ Hz is also reduced with a comparable factor.

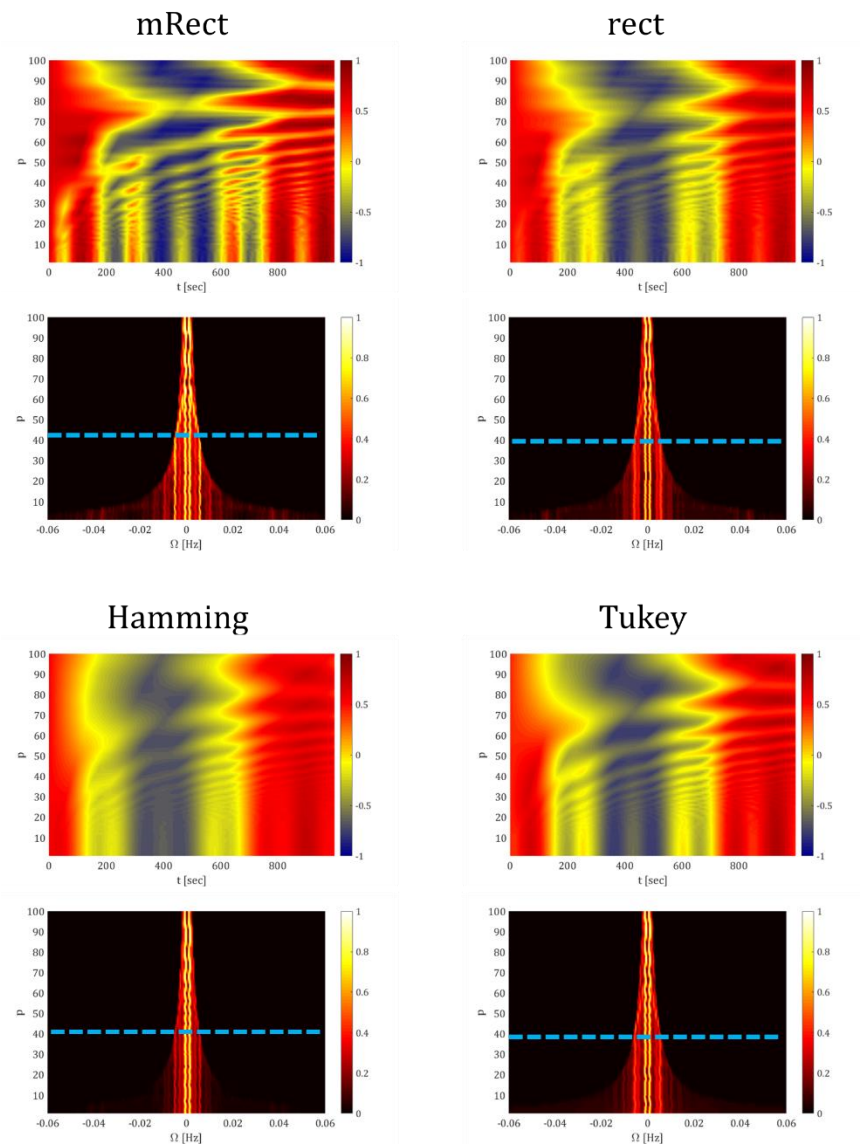

Figure S. 4. For each of the four window functions, the first row represents the SWC time series computed with different step sizes p, varied in the range of (1,100) with increments of 1 time point. The second row represents the frequency spectrum of the corresponding SWC time series computed with different step sizes. Increasing step size does not significantly affect the SWC time series (the first row) and frequency spectrum (second row), as long as it satisfied the proposed limit, i.e. $p \leq \Omega_s/2\Omega_c$. However, as step size increased beyond its upper bound limit, the SWC content underwent significant distortions (due to aliasing) as evident by the temporal profiles. In addition, frequency spectrums show how the higher frequency dynamic correlation, occurring at $\delta f_2 = 0.006$, was folded into the lower frequency content. For example, see the frequency spectrums, the value of p at which the occurrence of such distortions became clearly visible has been marked with a dashed line. Note that this results in strong low frequency components that do not represent the real dynamic correlations. In the first case, i.e. using mRect window, dynamic connectivity has strong

frequency component at 0.006 Hz, as opposed to the other 3 cases. Consequently, decreasing window bandwidth to below 0.006 Hz will affect the first case significantly while its effect on the other cases is less visible. It worth emphasizing that effect is not a drawback of using mRect window, and more importantly it again shows that mRect is capable of recovering high frequency components, while other windows fail.

Comparing windows using real fMRI data

To examine how the performance of the proposed window may differ from the conventional windows on real fMRI time series that lie in a wide frequency range, two regionally-averaged time series were extracted from a 10 minutes resting state fMRI scan, with $TR = 2$ sec and number of time points 300. For more information regarding data acquisition and preprocessing refer to (Mokhtari et al., 2018). This data was actually acquired in two separate resting state scanning runs (each of length 150 time points/ 5 minutes) in the same day and the same MRI data acquisition sessions. Here, to achieve a longer time series to compute reliable SWC connectivity and Fourier transformation, we concatenated the two scans after preprocessing that included band-pass filtering in the range of $(0.01, 0.1)$ Hz. The two regions included the posterior cingulate cortex (PCC) and left angular gyrus (AG) which have shown dynamic functional connection according to previous studies (Chang and Glover, 2010; Leonardi and Van De Ville, 2015). The SWC analysis was performed using different window functions with window length as suggested in the main document and step size of $p = 1$ time point.

For the two representative individual participants, we show the regional time series, the pointwise multiplication, the SWC time series and their frequency spectrum in Figure S. 4. For the first participant, as evident by the frequency spectrums, the mRect window showed superior performance in revealing the relative power of slower vs. faster dynamic correlations (e.g. the relative power of the component at 0.0005 vs. the components at 0.005 or 0.0065 Hz) compared to the conventional windows that failed to efficiently retrieve the amplitude of the faster dynamic correlations. Comparable observations were

also seen for the second representative participant, where the amplitude of the faster dynamic correlations (occurring over 0.004) were better captured by the mRect window.

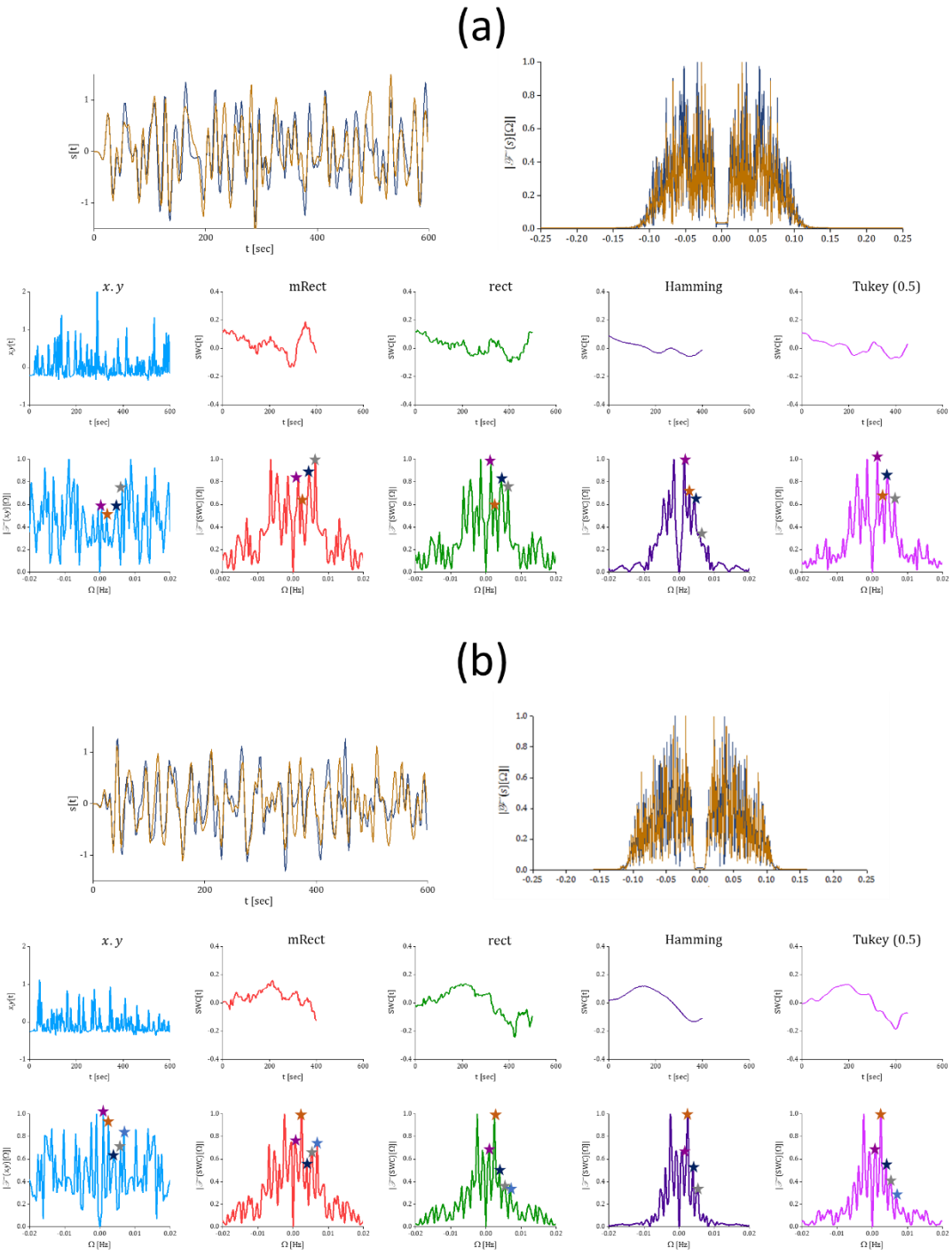

Figure S. 5. The PCC and AG time series (the first row) following the preprocessing, the pointwise multiplication and SWC time series and the frequency spectrums resulting from different window functions for two representative participants.

References

Chang, C., Glover, G.H., 2010. Time–frequency dynamics of resting-state brain connectivity measured with fMRI. Neuroimage 50, 81-98.

Leonardi, N., Van De Ville, D., 2015. On spurious and real fluctuations of dynamic functional connectivity during rest. Neuroimage 104, 430-436.

Mokhtari, F., Rejeski, W.J., Zhu, Y., Wu, G., Simpson, S.L., Burdette, J.H., Laurienti, P.J., 2018. Dynamic fMRI Networks Predict Success in a Behavioral Weight Loss Program among Older Adults. Neuroimage In press.